Dual-Band Polarization-Independent Subwavelength Grating Coupler for Wavelength Demultiplexing

Tianyi Hao, Alejandro Sánchez-Postigo, Pavel Cheben, Alejandro Ortega-Moñux, and Winnie N. Ye, *Senior Member, IEEE*

***Abstract*—Surface grating couplers are diffractive periodic structures that enable efficient coupling of light between optical fibers and planar waveguides. Conventional grating couplers have polarization specific and limited wavelength operation, because of the intrinsic radiation angle dependency on both wavelength and polarization. In this Letter, we propose, to the best of our knowledge, the first polarization-independent surface fiber-chip grating coupler, behaving as a wavelength splitter for the O and C communication bands. Polarization insensitivity is achieved by subwavelength segmentation of the silicon gratings, together with a novel design to allow the dual wavelengths to propagate along two opposite directions in the chip. For the TE and TM polarizations, coupling efficiencies around -4.5 dB are achieved at both 1310 nm and 1550 nm, with an average 1-dB bandwidth of ~45 nm and ~60 nm, respectively. This grating coupler concept can be used as a part of transceivers to increase the data rate of wavelength-division-multiplexing (WDM) systems for fiber-to-the-home (FTTH) network services.**

***Index Terms*—Grating coupler, dual-band, polarization independent, wavelength-division-multiplexing**

I. Introduction

SILICON photonics has emerged as one of the most popular research areas in integrated optics because of silicon's low cost and CMOS compatibility, and its natural oxidation process [1]. The high index contrast of the silicon-on-insulator (SOI) platform enables strong light confinement within the waveguide cores and leads to very compact devices, whose cross-section is much smaller than the diameter of conventional single-mode optical fibers. Surface grating couplers are key components to efficiently couple light from the chip to the optical fiber and vice versa. Unfortunately, conventional grating couplers have narrow spectral bandwidths and high polarization sensitivity due to the intrinsic dependency of the radiation angle with the wavelength and polarization [2]. In addition to fiber-chip coupling, surface grating couplers have been utilized as wavelength, polarization and power splitters [3-9]. Broadband and polarization-independent grating couplers have been designed to accommodate for the increasing communication speeds [10-12]. With a growing demand for wavelength-division-multiplexing (WDM) systems for the fiber-to-the-home (FTTH) network services, low-cost dual-band (O- and C-bands) transceivers are required, where dual-band grating couplers are one of the key elements to simplify the light coupling between the optical fibers and chips. Most dual-band designs work as wavelength multiplexer or demultiplexers [8, 12-15], with single-polarized light from two spectral bands being split into two waveguides to transmit in different directions. Alternatively, bi-wavelengths of different or same polarization have also been demonstrated to couple into the same direction [16-19]. Optimized devices based on inverse

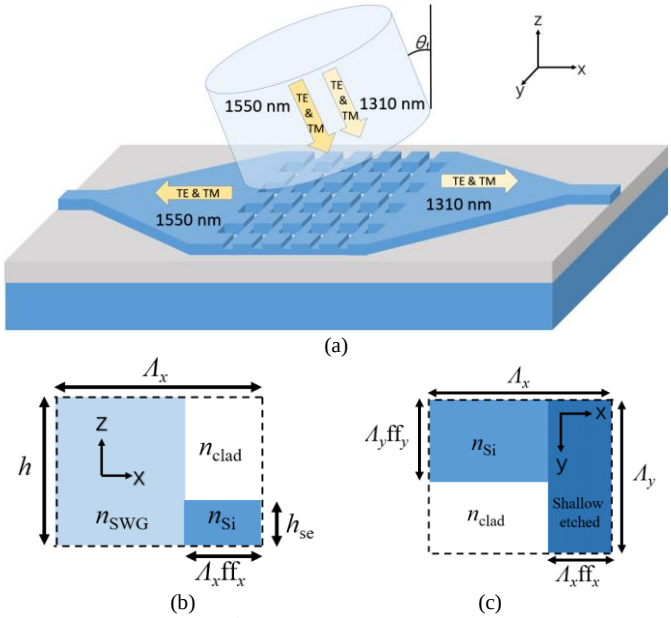

Fig. 1. (a) 3D schematic of the proposed dual-band polarization-independent grating coupler operating as a wavelength demultiplexer, with 1550-nm- and 1310-nm-wavelength light coupled out to the left and right ports, respectively. The actual grating will have a higher number of periods to efficiently radiate most of the power upward. The optical fiber is positioned on top of the grating with an off-vertical inclination angle θ_t. (b) Side view of a grating period. (c) Top view of a grating period.

Manuscript received ; accepted . Date of publication ; date of current version (*Corresponding author: Winnie N. Ye.*)

T. Hao and W. N. Ye are with the Department of Electronics, Carleton University, Ottawa, K1S 5B6, Canada. (e-mail: TianyiHao@cmail.carleton.ca; Winnie.Ye@carleton.ca).

A. Sánchez-Postigo and A. Ortega-Moñux are with the Dpto. Ingeniería de Comunicaciones, ETSI Telecomunicación, Universidad de Málaga, Málaga 2907, Spain. (e-mail: asp@ic.uma.es; aom@ic.uma.es).

P. Cheben is with the National Research Council Canada, Ottawa, K1A 0R6, Canada. (e-mail: Pavel.Cheben@nrc-cnrc.gc.ca).

Color versions of one or more of the figures in this letter are available online at http://ieeexplore.ieee.org.

Digital Object Identifier

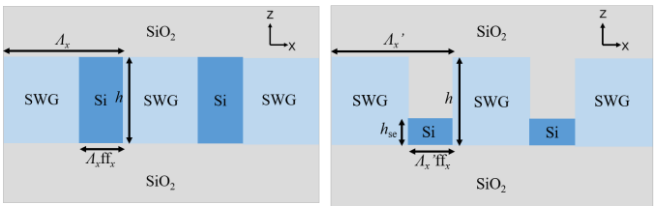

(a) (b)

Fig. 2. (a) Schematic representation of the grating structure used to achieve polarization insensitivity (lateral view)—first step of the design process. (b) Design steps to achieve dual-band-wavelength splitting while maintaining polarization insensitivity (lateral view)— shallow etch selection, h_{se}; and optimization of Λ_x to Λ_x'.

design and two-stage gradient-based optimization algorithms were reported [9, 13]; however, either moderate coupling efficiencies around -6 dB [12-17] or single-band operation [18, 19] performance was observed.

In this Letter, we propose a novel surface grating coupler that can operate, for the first time to the best of our knowledge, as a polarization-independent wavelength splitter (at 1310-nm and 1550-nm wavelengths). The input light of two wavelengths is coupled into the chip simultaneously from a single optical fiber, and is split and coupled out to two opposite output ports (see Fig. 1). Specifically, the polarization insensitivity and the wavelength splitting properties are achieved simultaneously by leveraging the index engineering of subwavelength metamaterials on a 360-nm-thick SOI platform. The presented work can pave the way toward more advanced WDM/FTTH systems by further increasing data rates and data capacities.

II. Design

Figure 1 illustrates a schematic of the proposed polarization-independent wavelength-splitting grating coupler. The device is designed on an SOI wafer with an upper silicon layer of thickness h and a buried oxide layer (BOX) of thickness h_{BOX}. The structure comprises a periodic waveguide of length $L = N_x\Lambda_x$ and width $W = N_y\Lambda_y$ ($W >> h$), where Λ_x and Λ_y are the period lengths or pitches in the x and y directions, respectively; and N_x and N_y are the corresponding numbers of periods. Each period in the propagation direction consists of a fully etched transverse subwavelength grating (SWG) region of length $\Lambda_x(1\text{-}ff_x)$ and a uniform shallow-etched silicon section of thickness h_{se} and length $\Lambda_x ff_x$, as shown in Fig. 1(b). The width of each silicon segment in the SWG section is given by the period Λ_y and the fill factor ff_y as depicted in Fig. 1(c). A silicon dioxide layer, not shown in the figure, is deposited on the top of the entire device to ensure structure integrity. Light beams at wavelengths of 1310 nm and 1550 nm are coupled from the optical fiber to the grating coupler, and are split into the right and left ports of the grating coupler, respectively. 500-μm-long linear adiabatic tapers were used to squeeze light efficiently from the grating to the interconnecting waveguides in the chip.

Radiation in conventional grating couplers is governed by the momentum conservation equation [20]:

$$\theta = \sin^{-1}\left(\frac{n_B}{n_c} + m\frac{\lambda}{n_c\Lambda_x}\right), \quad (1)$$

where θ is the radiation angle ($\theta = \theta_f$ for 1310 nm and $\theta = -\theta_f$ for 1550 nm in Fig. 1(a)), n_B is the effective index of the fundamental Bloch–Floquet mode supported by the grating, n_c is the refractive index of the cladding material (~ 1.44), m is an integer called 'diffraction order' (whose value is typically -1 [20]), λ is the operating wavelength and Λ_x is the period along the propagation direction. As the radiation angle depends strongly on the wavelength, conventional grating couplers cannot couple light from a fixed optical fiber into the chip with a broad bandwidth and therefore cannot operate efficiently in two different spectral bands. Similarly, because the Bloch–Floquet effective index for the TE mode is typically higher than that for the TM mode since the width W is much larger than the height h, conventional grating couplers couple light at a different angle for each polarization.

To overcome the wavelength and polarization intrinsic limitations of conventional surface grating couplers, we follow a three-step design strategy. Firstly, using the geometry in Fig. 2(a), polarization insensitivity is studied for each central wavelength by analyzing the thickness h, the fill factor of the grating in the propagation direction, ff_x, and the fill factor of the SWG region, ff_y. The engineering of refractive-index, dispersion, polarization and anisotropy can be effectively achieved in SWGs [21, 22]. In particular, SWG structures can make the effective indices of the TE and TM fundamental Bloch–Floquet modes in the grating coincide at a given wavelength λ_0 [10], such that

$$\theta_{TE}(\lambda_0) = \theta_{TM}(\lambda_0), \quad (2)$$

where θ_{TE} and θ_{TM} are the radiation angles associated to the TE and TM polarizations, respectively. Secondly, the shallow-etched structure is obtained by selecting h_{se}, as illustrated in Fig. 2(b), to engineer the effective indices at λ_0 = 1310 nm and λ_0 = 1550 nm, and to ensure that Eq. (2) is met at both wavelengths for a range of fill factors that are feasible for fabrication.

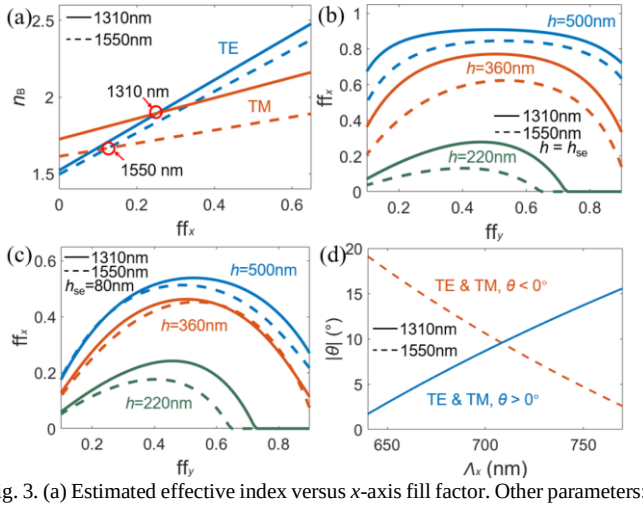

Fig. 3. (a) Estimated effective index versus x-axis fill factor. Other parameters: $h = h_{se}$ = 220 nm, ff_y = 0.35. The cross points between the curves at each wavelength (marked with red circles) show the x-axis fill factors that yield polarization insensitivity. (b) Estimated x-axis and y-axis fill factors that achieve polarization insensitivity for thickness $h = h_{se}$ = 220 nm, 360 nm and 500 nm. (c) Estimated x-axis and y-axis fill factors that achieve polarization insensitivity for thicknesses h_{se} = 80 nm and h = 220 nm, 360 nm and 500 nm. (d) Radiation angle (absolute value) as a function of the period Λ_x for TE and TM polarizations.

Finally, the period Λ_x is chosen and dimensions are refined via simulation to achieve

$$\theta(\lambda = 1310 \text{ nm}) = -\theta(\lambda = 1550 \text{ nm}) \quad (3)$$

while maintaining the polarization independence in Eq. (2). Equation (3) guarantees that light from an optical fiber with a fixed tilt angle $\theta_t = \theta(\lambda = 1310 \text{ nm})$ is coupled out to two opposite output waveguides, thereby enabling wavelength splitting.

As a first approximation, we analytically investigate the refractive index engineering of the SWG section, for the TE and TM polarizations, by using the second-order Effective Medium Theory (EMT), as shown in [10]. Then, we estimate the Bloch−Floquet effective index by

$$n_B = n_H \text{ff}_x + n_L (1 - \text{ff}_x), \quad (4)$$

where n_H and n_L denote the effective indices of the shallow-etched and SWG sections of the grating, respectively. Fig. 3(a) shows the calculated effective indices when $\text{ff}_y = 0.35$ and h = 220 nm at 1310-nm and 1550-nm wavelengths for TE and TM polarizations. A pitch Λ_y of 300 nm was chosen to ensure that the transverse periodic structure operates in the deep SWG regime with a minimum feature size greater than 100 nm. At each wavelength, the average effective index of the fundamental TE mode matches that of the TM mode for the specific x-axis fill factor, which corresponds to the cross point marked with a red circle in Fig. 3(a). Thus, for every ff_y, an ff_x value might exist that satisfies Eq. (2), which is represented in Fig. 3(b) for three different silicon thicknesses: h = 220 nm, h = 360 nm and h = 500 nm.

Clearly, regardless of the thickness h of the silicon layer and the pairs (ff_y, ff_x), it is impossible to achieve polarization insensitivity for both 1310-nm and 1550-nm wavelengths at the same time. We then introduce an additional degree of freedom (h_{se}), by allowing a shallow-etched (non-SWG) region of the grating, as shown in Fig. 2(b). With the shallow-etched segments, the difference in effective index between TE and TM modes can be successfully engineered to fulfill Eq. (2) for both λ_0 = 1310 nm and λ_0 = 1550 nm. As shown in Fig. 3(c), for h_{se} = 80 nm, h > 220 nm is required to realize polarization insensitivity at both central wavelengths. In order to choose the thicknesses of the fully and shallow-etched regions, two criteria are taken into consideration: (1) extreme fill factors might not be feasible in fabrication (e.g., for a chosen Λ_y of 300 nm, y-axis fill factors greater than 0.8 would imply a minimum feature size that is smaller than 60 nm, which is not suitable in typical deep-UV fabrication processes [23]); (2) thick silicon layers should be avoided to prevent multimode operation. Taking these conditions into account, a silicon thicknesses of 360 nm is selected in this preliminary design stage.

Finally, we utilize the grating equation Eq. (1) to find the period Λ_x that satisfies Eq. (3). The absolute value of the calculated radiation angle for both wavelengths is plotted as a function of Λ_x in Fig. 3(d), by forcing m = -1 as normally used in conventional grating couplers. The cross point between both curves, at θ = 9.6º, determines the optimal period that achieves wavelength splitting, Λ_x = 708 nm, while maintaining polarization insensitivity.

III. Simulation and Tolerance Analysis

We carried out three-dimensional finite-difference time-domain (3D FDTD) simulations using Lumerical FDTD to refine the dimensions previously estimated in the design stage [24]. An optical fiber was positioned over the grating with a tilt angle of 9º, from which a Gaussian field was launched for TE and TM polarizations, injecting wavelengths ranging from 1275 nm to 1335 nm in the C-band and 1510 nm to 1595 nm in the O-band. We calculate the amount of power coupled into their fundamental modes at each output waveguide. In order to run 3D simulations, the width of the grating coupler was scanned, revealing that the overlap between the radiated field and the fundamental mode of an SMF-28 optical fiber (mode field diameter of ~10 µm) is virtually independent of the width in the range 11–15 µm at both operating wavelengths. A final value of 13.2 µm (44 transverse periods) was chosen. The dimensions of the optimized device are summarized in Table I.

TABLE I
Structural Parameters of the Optimized Device

Axis	**Λ (nm)**	**# Periods**	**Fill factor**
x / y	735 / 300	13 / 44	0.385 / 0.56
h (nm)	**h_{se} (nm)**	**H_{BOX} (µm)**	**θ (º)**
360	80	2	9

The simulated coupling efficiencies (i.e., amount of power coupled to the correct port) and crosstalks (i.e., amount of power coupled out to the opposite port) for each polarization and spectral band are shown in Fig. 4, where 1-dB bandwidths ($BW_{1\text{-dB}}$) are labeled. For all peak wavelengths (λ ~ 1310 nm and λ ~ 1550 nm) and polarizations (TE and TM), a coupling efficiency around -4.5 dB (~35%) is predicted, as well as a crosstalk of less than -20 dB (1%). The FDTD-simulated performance metrics are extracted and summarized in Table II.

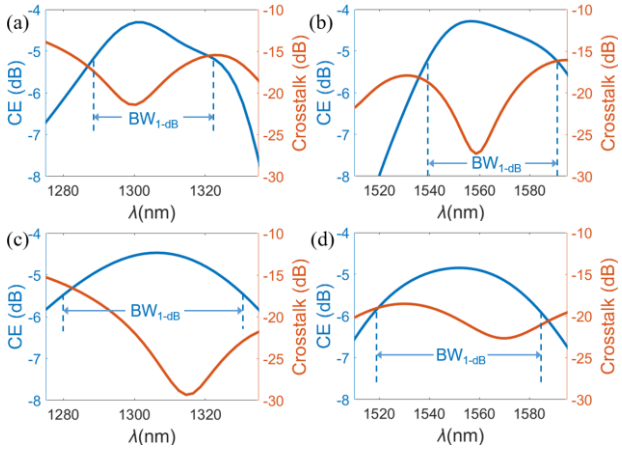

Fig. 4. Simulated coupling efficiency and crosstalk as a function of the wavelength for (a) O-band [TE], (b) C-band [TE], (c) O-band [TM] and (d) C-band [TM].

TABLE II
Simulated Coupling Efficiency and 1-dB Bandwidth

Wavelength, polarization	**Coupling Efficiency**	**1-dB bandwidth**
C-band, TE / TM	-4.3 dB / -4.9 dB	54 nm / 65 nm
O-band, TE / TM	-4.3 dB / -4.5 dB	38 nm / 53 nm

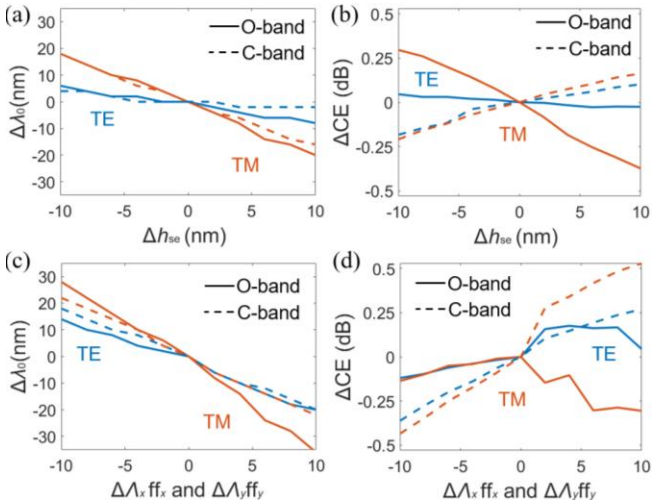

Fig. 5. Tolerance analysis of the designed device. (a) Central wavelength and (b) coupling efficiency deviation as a function of errors in the shallow-etched depth. (c) Central wavelength and (d) coupling efficiency deviation as a

Two steps are required to fabricate the proposed grating coupler: to define fully etched SWG sections and to shallow-etch the silicon sections. In Fig. 5, we study the influence of fabrication deviations in the etch depth (Δh_{se}) and the size of grating teeth ($\Delta\Lambda_x ff_x$ and $\Delta\Lambda_y ff_y$ simultaneously) with respect to the nominal values, using 3D FDTD. Fabrication errors lead to a maximum wavelength shift $\Delta\lambda_0$ of ±35 nm with respect to the central operating wavelengths of the grating couplers [Figs. 5(a) and 5(c)], while the degradation of the coupling efficiency (|ΔCE|) is less than 0.52 dB (~4.2%) in all cases. As expected, mask misalignments of ±20 nm have a higher influence on the device's performance [25], with an additional overall degradation in the coupling efficiency of around 1.7 dB.

IV. Conclusion

In this Letter, a novel polarization-independent wavelength-splitting surface grating coupler concept on a 360-nm-thick silicon-on-insulator platform for the O and C communication bands has been presented. Coupling efficiencies around -4.5 dB (~35%) and 1-dB bandwidths around 50 nm are achieved for both bands and polarizations. A detailed fabrication tolerance analysis was included to demonstrate the performance impact due to fabrication variations. The reported results show that polarization independency and wavelength demultiplexing can be achieved simultaneously in SOI. Further research to accomplish the practical application of the proposed grating couplers could involve the utilization of more complex SWG structures in standard SOI platforms. We believe this work benefits the development of wavelength-division-multiplexing systems with multiple channels for fiber-to-the-home services and open new venues for the investigation of advanced grating coupling schemes.

References

[1] X. Chen et al., "The emergence of silicon photonics as a flexible technology platform," Proc. IEEE, vol. 106, no. 12, pp. 2101–2116, Dec. 2018.

[2] S. Nambiar, P. Sethi, and S. Selvaraja, "Grating-Assisted Fiber to Chip Coupling for SOI Photonic Circuits," Appl. Sci., vol. 8, no. 7, p. 1142, Jul. 2018.

[3] Z. Cheng, X. Chen, C. Y. Wong, K. Xu, and H. K. Tsang, "Apodized focusing subwavelength grating couplers for suspended membrane waveguides," Appl. Phys. Lett., vol. 101, no. 10, p. 101104, Sep. 2012.

[4] Xia Chen and H. K. Tsang, "Nanoholes Grating Couplers for Coupling Between Silicon-on-Insulator Waveguides and Optical Fibers," IEEE Photonics J., vol. 1, no. 3, pp. 184–190, Sep. 2009.

[5] D. H. Raguin and G. M. Morris, "Antireflection structured surfaces for the infrared spectral region," Appl. Opt., vol. 32, no. 7, pp. 1154–1167, Mar. 1993.

[6] R. Halir, P. Cheben, S. Janz, D.-X. Xu, Í. Molina-Fernández, and J. G. Wangüemert-Pérez, "Waveguide grating coupler with subwavelength microstructures," Opt. Lett., vol. 34, no. 9, pp. 1408–1410, May 2009.

[7] Y. Wang et al., "Design of broadband subwavelength grating couplers with low back reflection," Opt. Lett., vol. 40, no. 20, pp. 4647–4650, Oct. 2015.

[8] G. Roelkens, D. Van Thourhout, and R. Baets, "Silicon-on-insulator ultra-compact duplexer based on a diffractive grating structure," Opt. Express, vol. 15, no. 16, pp. 10091–10096, 2007.

[9] J. Feng and Z. Zhou, "Polarization beam splitter using a binary blazed grating coupler," Opt. Lett., vol. 32, no. 12, pp. 1662–1664, Jun. 2007.

[10] X. Chen and H. K. Tsang, "Polarization-independent grating couplers for silicon-on-insulator nanophotonic waveguides," Opt. Lett., vol. 36, no. 6, pp. 796–798, Mar. 2011.

[11] S. Shao and Y. Wang, "Highly compact polarization-independent grating coupler," Opt. Lett., vol. 35, no. 11, pp. 1834–1836, Jun. 2010.

[12] L. Su, R. Trivedi, N. V. Sapra, A. Y. Piggott, D. Vercruysse, and J. Vučković, "Fully-automated optimization of grating couplers," Opt. Express, vol. 26, no. 4, pp. 4023–4034, Feb. 2018.

[13] A. Y. Piggott, J. Lu, T. M. Babinec, K. G. Lagoudakis, J. Petykiewicz, and J. Vučković, "Inverse design and implementation of a wavelength demultiplexing grating coupler," Sci. Rep., vol. 4, no. 1, p. 7210, May 2015.

[14] L. Cheng, X. Mu, S. Wu, X. Tu, and H. Y. Fu, "Perfectly Vertical Grating Coupler for O and C-band," in Frontiers in Optics + Laser Science APS/DLS, 2019, p. JW4A.57.

[15] J. Tan, H. Pang, F. Meng, and J. Jiang, "Compact and high-efficient wavelength demultiplexing coupler based on high-index dielectric nanoantennas," Chinese Phys. B, vol. 27, no. 9, p. 094217, Sep. 2018.

[16] S. Nambiar, H. Muthuganesan, T. Sharma, and S. K. Selvaraja, "On-chip unidirectional dual-band fiber-chip grating coupler in silicon nitride," OSA Contin., vol. 1, no. 3, pp. 864–871, Nov. 2018.

[17] M. Streshinsky et al., "A compact bi-wavelength polarization splitting grating coupler fabricated in a 220 nm SOI platform," Opt. Express, vol. 21, no. 25, pp. 31019–31028, Dec. 2013.

[18] W. Zhou, Z. Cheng, X. Sun, and H. K. Tsang, "Tailorable dual-wavelength-band coupling in a transverse-electric-mode focusing subwavelength grating coupler," Opt. Lett., vol. 43, no. 12, pp. 2985–2988, Jun. 2018.

[19] W. Zhou and H. K. Tsang, "Dual-wavelength-band subwavelength grating coupler operating in the near infrared and extended shortwave infrared," Opt. Lett., vol. 44, no. 15, pp. 3621–3624, Aug. 2019.

[20] T. Tamir and S. T. Peng, "Analysis and design of grating couplers," Appl. Phys., vol. 14, no. 3, pp. 235–254, Nov. 1977.

[21] P. Cheben, R. Halir, J. H. Schmid, H. A. Atwater, and D. R. Smith, "Subwavelength integrated photonics," Nature, vol. 560, no. 7720, pp. 565–572, Aug. 2018.

[22] R. Halir et al., "Subwavelength-grating metamaterial structures for silicon photonic devices," Proc. IEEE, vol. 106, no. 12, pp. 2144–2157, Dec. 2018.

[23] P. J. P. Chausse, E. D. Le Boulbar, S. D. Lis, and P. A. Shields, "Understanding resolution limit of displacement Talbot lithography," Opt. Express, vol. 27, no. 5, pp. 5918–5930, Mar. 2019.

[24] "Nanophotonic FDTD Simulation Software - Lumerical FDTD," Lumerical. [Online]. Available: https://www.lumerical.com/products/fdtd/.

[25] M. Kamandar Dezfouli et al., "Perfectly vertical surface grating couplers using subwavelength engineering for increased feature sizes," Opt. Lett., vol. 45, no. 13, pp. 3701–3704, Jul. 2020.